VILNIUS UNIVERSITY

CENTER FOR PHYSICAL SCIENCES AND TECHNOLOGY

MILDA TAMOŠIŪNAITĖ

IMPACT OF EXTERNAL EFFECTS ON TERAHERTZ APPLICATIONS FOR TELECOMMUNICATIONS

Summary of doctoral thesis

Physical Sciences, Physics (02P)

Vilnius, 2018

The research has been carried out in 2012 - 2018 at the Center for Physical Sciences and Technology.

Scientific supervisor – prof. dr. Gintaras Valušis (Center for Physical Sciences and Technology, Physical sciences, Physics – 02P).

Dissertation will be defended in the united Vilnius University and Center for Physical Sciences and Technology Council of Physical sciences:

Chairman – prof. dr. Nerija Žurauskienė (Center for Physical Sciences and Technology, Physical sciences, Physics – 02P).

Members:

Doc. dr. Rimvydas Aleksiejūnas (Vilnius University, Physical sciences, Physics – 02P);

Dr. Vaidas Pačebutas (Center for Physical Sciences and Technology, Physical sciences, Physics – 02P);

Dr. Šarūnas Meškinis (Kaunas University of Technology, Physical sciences, Physics – 02P);

Prof. habil. dr. Kęstutis Staliūnas (Polytechnic University of Catalonia, Physical sciences, Physics – 02P).

The dissertation will be defended under open consideration in the Council of Physical sciences on 28th September, 2018, 10 a.m. at the Center for Physical Sciences and Technology, room D401.

Address: Saulėtekio ave. 3, LT-10257, Vilnius, Lithuania.

The summary of the dissertation was distributed on August 28, 2018.

The dissertation is available in Vilnius University, Center for Physical Sciences and Technology libraries and in VU web site: *www.vu.lt/lt/naujienos/ivykiu-kalendorius*.

VILNIAUS UNIVERSITETAS

FIZINIŲ IR TECHNOLOGIJOS MOKSLŲ CENTRAS

MILDA TAMOŠIŪNAITĖ

IŠORINIO POVEIKIO ĮTAKA TERAHERCŲ TAIKYMAMS TELEKOMUNIKACIJOSE

Daktaro disertacijos santrauka

Fiziniai mokslai, fizika (02P)

Vilnius, 2018 metai

Disertacija rengta 2012 – 2018 metais Fizinių ir technologijos mokslų centre.

Mokslinis vadovas - prof. dr. Gintaras Valušis (Fizinių ir technologijos mokslų centras, fiziniai mokslai, fizika – 02P).

Disertacija ginama viešame disertacijos Gynimo tarybos posėdyje:

Pirmininkė – prof. dr. Nerija Žurauskienė (Fizinių ir technologijos mokslų centras, fiziniai mokslai, fizika — 02P).
Nariai:
Doc. dr. Rimvydas Aleksiejūnas (Vilniaus universitetas, fiziniai mokslai, fizika – 02P);
Dr. Vaidas Pačebutas (Fizinių ir technologijos mokslų centras, fiziniai mokslai, fizika – 02P);
Dr. Šarūnas Meškinis (Kauno technologijos universitetas, fiziniai mokslai, fizika – 02P);
Prof. habil. dr. Kęstutis Staliūnas (Katalonijos politechnikos universitetas, fiziniai mokslai, fizika – 02P).

Disertacija bus ginama viešame disertacijos Gynimo tarybos posėdyje 2018 m. rugsėjo 28 d. 10 val. Fizinių ir technologijos mokslų centro D401 auditorijoje.

Adresas: Saulėtekio al. 3, LT-10257, Vilnius, Lietuva.

Disertacijos santrauka išsiuntinėta 2018 m. rugpjūčio mėn. 28 d.

Disertaciją galima peržiūrėti Vilniaus universiteto, Fizinių ir technologijos mokslų centro bibliotekose ir VU interneto svetainėje adresu:
www.vu.lt/lt/naujienos/ivykiu-kalendorius

Acknowledgement

I am sincerely grateful to my scientific supervisor prof. Gintaras Valušis for the opportunities, ideas, valuable advices and comprehensive support.

I am also thankful to the co-authors of the publications and colleagues from the Terahertz Photonics Laboratory. It is a great honour for me to have an opportunity to work with all of you.

I thank my family for the support and patience.

Introduction

In recent years, world mobile data traffic is growing nearly exponentially. Rates have doubled every eighteen months over the last three decades, and are quickly approaching the capacity of wired communication systems [1]. Therewith, further growth is expected [2]. Available bandwidth is one of the factors limiting data transmission rate [3]. Therefore, the fifth generation microwave-based mobile network (5G) is being developed. However, current wireless technologies, coupled with the new 5G technology, is expected to meet only 81 percent of the planned need [4]. This limit and allocation of frequency ranges to specific applications would restrict the future growth of wireless communications unless new frequency ranges are exploited. One of the promising candidates is the Terahertz (THz) Band, which is defined as electromagnetic waves in the frequency region of 100 GHz – 10 THz [5]. One terahertz (1 THz = 10^{12} Hz) corresponds to a vacuum wavelength of 300 μm. Wide up to 120 GHz spectrum bands with relatively low atmospheric absorption can be found in these ranges. Therefore, availability of unallocated bandwidth in sub-terahertz (sub-THz; 0.1 – 0.3 THz) and THz ranges together with a fast development of system components [6], [7] spurred a rapid research of THz applications in communications (hereinafter - B5G, *Beyond 5G*). Since the THz waves are very vulnerable in the Earth's atmosphere, the best performance of the THz wireless networks was shown under in-door conditions [8]. However, THz communications could benefit from the main principles of the 5G (short distances, infrastructure densification, beamforming, multiple-input multiple-output (MIMO) antenna arrays, consisting of tens or hundreds of antennas) [9] and well-developed fiber-optics links (i.e., wireless-over-fiber technology for the difficult to access areas) [10].

In this work, the possibilities and limitations of the THz wireless networks were examined in terms of the atmospheric attenuation, mostly rain attenuation and variations of atmospheric refractive index. Also, one of the most probable technological scenarios (short distances and quasi-optical transmission) was investigated. The results were compared with data from a laboratory-controlled rain experiment [11]. Since most of the existing equipment used in the industry is not designed to perform calibrated

measurements of the 5G/B5G wireless networks in air [12], such experiments can be used to predict the expected data transfer performance.

However, simulation of atmospheric attenuation is just one of the steps in the development of the THz telecommunications. Its components are also equally important. Budged analysis of the THz wireless systems revealed that better transmitter and/or receiver are required together with at least 100 dBi/km antenna gains [10]. Therefore, in order to overcome small gain and effective area of individual THz Band antennas, very large antenna arrays will be required [13]. The planar zone plate (ZP) lenses display benefit of being much smaller in depth, volume and weight than the ordinary lenses used in antennas [14]. Therefore, zone plate-based antennas are considered as a reduced size and cost, easy-integrated planar solution for telecommunication systems in millimeter-wave and THz bands [14], [15], [16], [17].

One of the tasks of this work was to simulate a compact laser-ablated focusing optical element for the THz Band (0.6 THz frequency), combining the reflection-reducing and phase-shifting properties. Prototype binary zone plate with a dual function antireflective (AR) layer (alternating rings with either flat or structured surface formed on one side, and fully structured on the other side of the silicon wafer of 500 μm thickness) was produced. Improved suitability for integration into compact optical components formed within relatively thin semiconductor substrates are revealed. Focusing performance of such binary ZP with dual function AR layer is close to the diffraction limited operation.

Main goal

The aim of this work was to evaluate peculiarities of THz electromagnetic wave propagation loss in contemporary and future wireless communication systems under real-time atmospheric conditions and to offer integrated, reflection-reducing and focusing passive component for THz communication systems.

Objectives

1. Theoretical investigation of the influence of instantaneous rainfall intensity values and variations of the atmospheric refractive index on attenuation of the THz waves propagating in the atmosphere.
2. Evaluation of the impact of random fluctuations of attenuation due to rain on the propagation of THz waves in case of the B5G technology.
3. Theoretical validation of the reflection-reducing structured layers' designs, optimized for production using laser-ablation method.
4. Study of the phase shift peculiarities in the reflection-reducing layers and investigation of the possibilities to use them in the formation of focusing elements directly on the semiconductor substrates.

Novelty

The significance of the changes in the instantaneous rain-rate values and the atmospheric refractive index was demonstrated by analysing the atmospheric attenuation of sub-THz (100 GHz) and THz (300 GHz) frequencies using real-time data. It has been shown that the averaged rain-rate values distorted the simulation results of the heavy rain event (high instantaneous rain-rate values decreased, small values increased, and the peak attenuation shifted in time). In addition, it has been demonstrated that in the area of poor coverage changes of the signal strength occurred at the same time as the variations of atmospheric refractive index.

For the first time, the attenuation fluctuations for the THz Band in case of short distances and quasi-optical transmission (expected in the THz-based B5G networks) were consistently evaluated and compared to the laboratory-based-experiments.

The reflection-reducing structures were consistently optimized and produced using laser-ablation technology, and the phase-shifting properties of those structures were investigated. The phase-shifting possibilities were employed for the zone plate design, in

which reflection-reducing and focusing features are compatible and all of this comes on one 500 μm thick silicon substrate[1].

The practical value

Since most of the existing industrial equipment is not designed to perform calibrated measurements of the 5G/B5G wireless networks over-the-air, accurate evaluation of the instantaneous rain-rate values and variations of the atmospheric refractive index would help to improve the evaluation of the connection quality. In addition, studies of the THz radiation in the rain will allow a better assessment of not only (already standardized and well understood) calculations of the average attenuation coefficient, but also expected deviations in the case of short distances and quasi-optical transmission.

As a result of phase shifts in the laser-ablated reflection-reducing structures, suggested zone plates could replace the currently used high-resistivity silicon (HR-Si) lenses and, in comparison, provide smaller losses on the surfaces, thus improving the signal-to-noise ratio and avoiding strong parasitic reflections from the surfaces of the focusing elements. Implementation of the sub-THz/THz communication systems may require large antenna arrays. The zone plates are more compact optical elements than the standard lenses. This feature would reduce antenna dimensions.

Statements to defend

1. Modelling of the electromagnetic wave attenuation in the atmosphere in the case of the 5G/B5G networks, requires the instantaneous (“one minute”) rain-rate and refractive index values, since averaged data may lead to significant deviations from the real values.

[1] Works in this field: C. Kadlec et al (2008), Y. W. Chen et al (2009), Y. W. Chen and X. Zhang (2014), A. Brahm et al (2014), O. Yurduseven et al (2016), N. T. Nguyen et al (2008), N. T. Sönmez and N. T. Tokan (2016), T. Nitta et al (2017).

2. Due to the quasi-optical transmission and relatively short distances of the 5G/B5G wireless networks (in relation to today's wireless communications), attenuation deviations can be noticeable from values based on today's standardized models.
3. In the reflection-reducing layers, where the period of the structure is close to the incident wavelength, it is possible to produce a thinner antireflective layer and to ease the production of the layers using laser-ablation method, still maintaining a small reflection coefficient.
4. Phase shifts in such structured reflection-reducing layers made of silicon are sufficiently well controlled, therefore, high quality focusing elements could be obtained for both THz telecommunication and THz imaging systems allowing to reach close to diffraction limited operation.

Contribution of the author

The author performed numerical simulations, prepared manuscripts related to the topic of the doctoral thesis, participated in the preparation of reports for conferences and presented some of them herself.

Contribution of the co-authors of the publications: the ablation of reflection-reducing coatings and zone plates was carried out at the FTMC Laser Research Department by dr. S. Indrišiūnas and dr. G. Račiukaitis. The Terahertz time-domain spectroscopy (THz-TDS) and THz imaging experiments were performed with dr. L. Minkevičius. All co-authors of the articles contributed by editing the manuscripts and preparing the articles for press.

The summary of doctoral thesis is organized as follows

Chapter 1 describes main mechanisms of the atmospheric attenuation, discuss in details impact of rain attenuation and variations of the atmospheric refractivity. It also presents simulations using real-time data. Chapter 2 is dedicated to the simulations using classical scattering theory. Finally, Chapter 3, considers optimization and investigation of reflection-reducing and focusing as well as phase-shifting structures for THz communication systems, fabricated using laser-ablation.

1. Atmospheric attenuation

1.1. Atmospheric composition and attenuation mechanisms

In the atmosphere, due to presence of the constituent gases and water droplets, attenuation of the propagating electromagnetic waves occurs. Some of the energy is absorbed due to resonant frequencies of the gas molecules, some is scattered by water particles. Some aerosols are very important for the condensation of water vapour, which in turn form water drops. In addition, the free-space loss (FSL) [18] is always present; therefore, the signal strength is constantly decreasing as the distance increases. Furthermore, due to variations of the atmospheric refractive index, anomalous propagation, fading and phase-front distortions might occur [6].

Oxygen and highly variable water vapour molecules are the main contributors to the gaseous attenuation. In the molecular absorption spectrum [19], [20], there are several regions of relative transparency between the absorption peaks, called transmission windows. Under standard atmospheric conditions, transmission windows are present at about <0.300, 0.330–0.370, 0.390–0.440, 0.625–0.725, and 0.780–0.910 THz [21], and the absorption above 1 THz is critical [10]. The effect due to water droplets depends on the type of the phenomenon (i.e., rain, fog). The effect due to rain is severe for frequencies above 10 GHz [22]. The attenuation due to fog is proportional to frequency. For example, at 300 GHz fog can be treated as a light rain, and at about 1 THz the attenuation due to fog exceeds attenuation due to heavy rain [23]. The atmospheric refractive index is defined as the ratio of the velocity of propagation of a radio wave in free space to the velocity in a specified medium. At standard atmosphere conditions near the Earth's surface, the radio refractive index has a value of approximately $n = 1.0003$. Changes in pressure, temperature and density affect the value of the atmospheric refractive index and its gradient.

The design techniques of the new telecommunication links take into account a series of various factors that are comprehensively explained by Freeman [22] and regulated by the International Telecommunication Union (ITU).

1.2. Empirical and physical design techniques of the rain attenuation

Averaged attenuation of THz radiation due to rain could be evaluated using relatively simple empirical model [24], where the power-law relationship between the rain-rate R (mm/h) and the specific attenuation A_R (dB/km) is:

$$A_R = kR^{\xi}, \tag{1}$$

where values for the coefficients k and ξ are determined as functions of frequency, f (GHz), in the range from 1 to 1 000 GHz. These functions and other needed values for both vertical and horizontal polarizations are given in ITU recommendation [24]. As it will be shown further, the challenging part of its application is evaluation of the reliable rain-rate value.

However, this simplified approach is only one of the available alternatives. The other group of the design techniques are physical methods. It is a common practice to express the excess attenuation due to rainfall as a function of the rain-rate, which depends on liquid water content and the fall velocity of the raindrops, which in turn depends on drop size distribution (DSD). There are various raindrop size distributions. Dealing with DSD is a complex task, because the shapes of actual raindrops are far from the usually depicted spherical or tear-drop shapes, as larger drops become flattened and eventually break into smaller droplets [25]. There are various raindrop size distributions. In this work, Weibull raindrop-size distribution will be used, since it provides the best percentage of the most successful approximations of raindrop-size distributions [26] and is one of the most relevant THz attenuation approximations [27], [28].

1.3. Rainfall simulations using real-time data

A. The annual rain-rate value

An analysis of long-term rainfall data revealed that heavy rain in Lithuania can be expected from May to September, therefore, the adjusted Rice and Holmberg model [29] was proposed in [IP9]:

$$R_{(1\text{ min.})} = \frac{\ln\left(0.0144\frac{M_{\text{V–IX}}}{t}\right)}{0.03}, \tag{2}$$

where $M_{\mathrm{V-IX}}$ is an amount of rainfall (mm), which fell in the area between May and September, t is the number of hours per year when the rain intensity can be equal or exceed $R_{(1\ \mathrm{min.})}$ value (for example, when the reliability of the system should be 99.99%, the $R_{(1\ \mathrm{min.})}$-value can be equal to or exceeded only 0.01% of the time of the year).

According to Eq. (2) and long-term meteorological data, in Lithuania the $R_{(1\ \mathrm{min.})}$-value is equal to 60.23 mm/h [IP7]. It is twice the ITU recommended value. However, instantaneous rain-rate values can be even higher. Therefore, one of the main challenges of the radio system design is the reliable sources of data.

B. The rain-rate of the heavy-rain event

In Figure 1, the data of the heavy-rain event are presented. During 6-h lapse, the rain intensity differed from light to heavy rain, and 37 mm of rain was accumulated until midnight (marked as vertical bars and "(mm)"). At the same time, the rain-rate was measured using WS1080 local weather station. For technical reasons, the measurements were carried out in 10-min intervals. In addition, 10-min rain rate values were converted to 1-min values, using the Moupfouma and Martin method[2] [30]. According to measurements, the maximum R-value was $R = 59.4$ mm/h at 20:49. However, the calculated 1-min R-value was almost double, $R_{1\mathrm{min}} = 103.45$ mm/h. Both of these values were higher than the ITU-R suggested value $R = 35$ mm/h.

[2] Please note, that the Rice and Holmberg model (Eq. (2)) was suggested for evaluation of the rain rate value exceeded non more than specified threshold of the year. The Moupfouma and Martin method, $R_{(1\ \mathrm{min})} = \left(R_{(\tau_{\mathrm{min}})}\right)^{0{,}987\tau_{\mathrm{min}}^{0{,}061}}$ (τ is a time interval between measurements), was used for conversion of individual 10-min rain rate values to individual 1-min rain rate values.

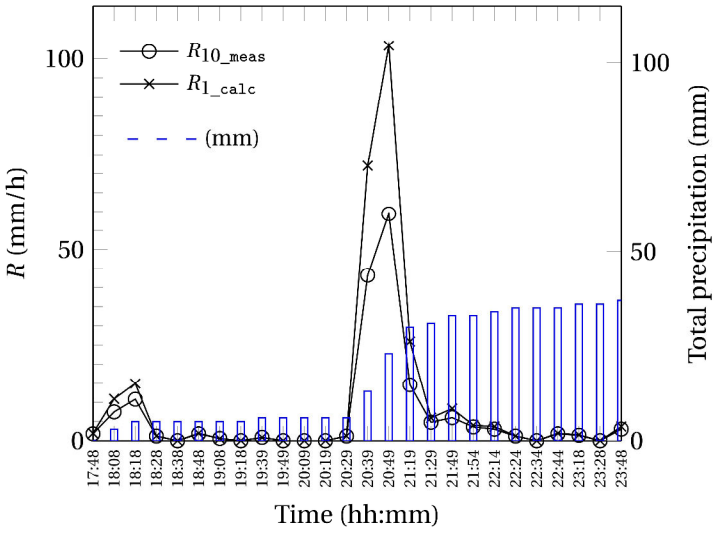

Figure 1. The heavy-rain event [PS1].

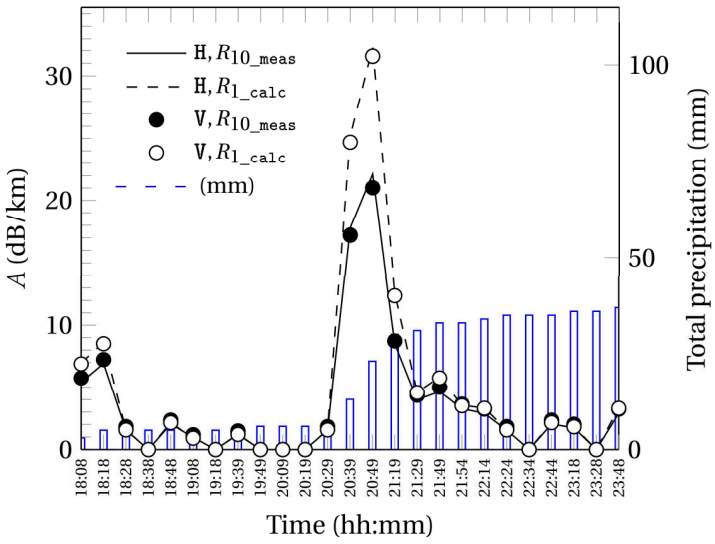

Figure 2. The calculated values of rain attenuation at 0.1 THz, using real-time R-values of the heavy-rain event (1- and 10-min integration time; horizontal (H) and vertical (V) polarization) [PS1].

Calculated values of rain attenuation (using Eq. (1)) at 0.1 THz are presented in Figure 2. As can be seen, the results are different for 1- and 10-min integration time (time intervals between rain-rate measurements, τ). 1-min rain-rate value ("R_{1_calc}") reveals the peak attenuation being 32.27 dB/km for horizontally (H) polarized waves and 31.55 dB/km for vertically (V) polarized ones. The values calculated using 10-min ("$R_{10_{meas}}$") integration time are lower (22.11 and 21.02 dB/km, respectively). When the rain rate starts to fall, the results in both cases are nearly similar.

In Figure 3, the same heavy-rain event is presented. The difference is that the R-values were calculated using more widely accessible averaged rainfall data with integration time of 1 h and 6 h. It can be seen that the results are distorted: since the downpours are suppressed and delayed ($R = 24.6$ mm/h at 21:19 according to hourly data, $R = 6.56$ mm/h at 23:18 according to 6-h average data (both not seen in the figure)), the low attenuation values become higher, and the peak values become lower (12.13 dB/km for horizontally polarized waves in comparison with 32.27 dB/km in Figure 2). The 6-h R-values determine low and almost constant (3-5 dB/km) attenuation values.

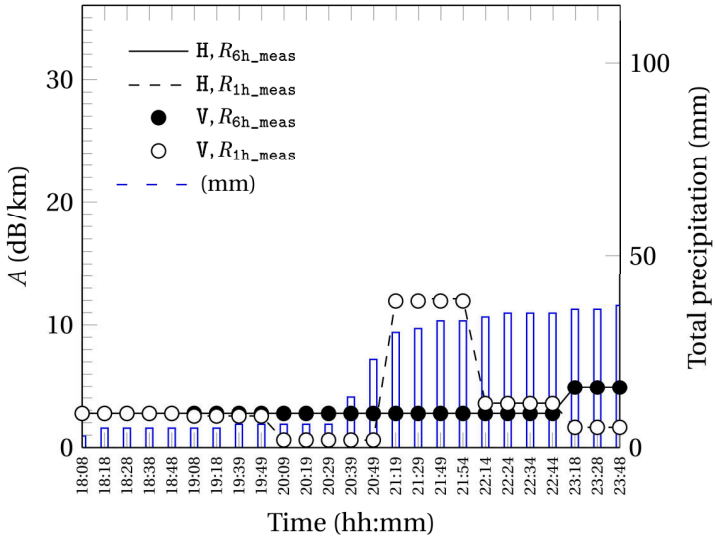

Figure 3. The calculated values of rain attenuation at 0.1 THz, using real-time R-values of the heavy-rain event (1- and 6-h integration time) [PS1].

The same calculations were performed for 0.3 THz (or 300 GHz; in many cases, this frequency is considered as a realistic candidate for the THz communications, and a starting point for power budget analysis). The main tendencies are the same as for 0.1 THz, however, calculated attenuation values are smaller (1-min value is about 30 dB/km (30.22 dB/km for horizontally polarized waves and 29.75 dB/km for vertically polarized ones), 10-min values are about 21 dB/km (21.31 dB/km and 21.02 dB/km respectively)). According to the ITU model [24], the rain attenuation values begin to slightly decrease at about 0.25 THz and asymptotically approach a straight line. One of the possible reasons

behind this is the change of scattering mechanism from Mie to non-selective scattering (it occurs when the particle sizes become much larger than the wavelength; non-selective scattering affects the entire spectrum equally [31]).

1.4. Variations of the atmospheric refractive index and its gradient

The atmospheric refractive index, n, can be calculated by the following formula:

$$n = 1 + N \cdot 10^{-6}, \tag{3}$$

here N is atmospheric refractivity (in *N*-units).

Since changes are observed in the fourth or fifth decimal places, it is more convenient to observe the changes of the N-value. According to the procedures described in [32] and [22], the N-value can be calculated as a function of temperature, atmospheric pressure and partial vapour pressure:

$$N = \frac{77.6}{T}\left(P + 4810\frac{e}{T}\right), \tag{4}$$

here P is atmospheric pressure (hPa), T is absolute temperature (K), e is water vapor pressure (hPa). Since there is no frequency dependence in Eq. (4), and the expression is considered to be true up to 100 GHz [22], the results should be suitable for the sub-THz frequencies.

The refractivity changes in the vertical direction can be restated in the terms of gradient, G (*N*-units/km):

$$G_N = \frac{\Delta n}{\Delta h} = \frac{\Delta N}{\Delta h}(10^{-6}), \tag{5}$$

$$\frac{\Delta N}{\Delta h} = \frac{N_1 - N_2}{h_1 - h_2}, \tag{6}$$

here N_1 and N_2 are atmospheric refractivities above ground at the heights of h_1 and h_2.

The refractivity gradient is an important parameter since it determines the type of the atmospheric refraction, which in turn determines how the travelling electromagnetic wave will bend. The G-value from 0 to -79 *N*-units/km means that the refraction is normal; -40 *N*-units/km is the value of the standard refraction; from -79 to -157 *N*-units/km is the

condition of the super-refraction (the situation when the propagating signal is bending towards ground); below -157 *N*-units/km is ducting (the atmosphere turns into waveguide, therefore there are some "dead zones" outside of it).

On the basis of averaged multiannual data[3], the annual, seasonal and daily values of the atmospheric refractivity were evaluated [IP8], [IP5], using Eq. (4). The results are presented in Figure 4. It can be seen that on average the *N*-value increases in the summer months, also, the highest value is in the morning, and the lowest in the evening.

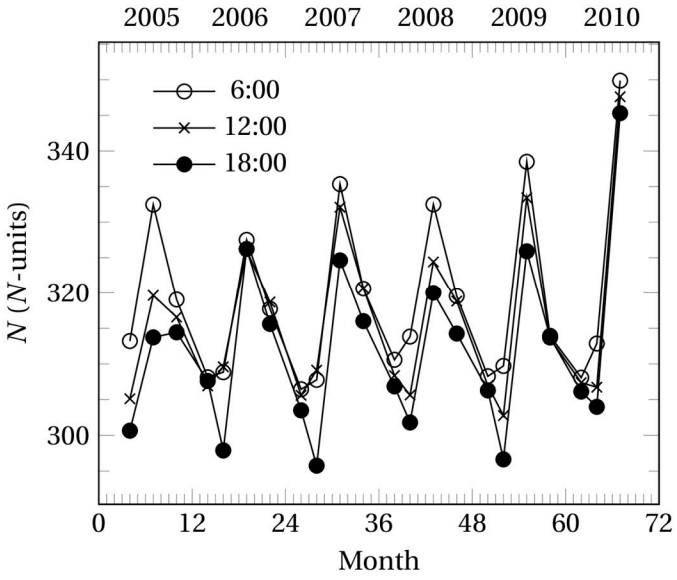

Figure 4. Annual, seasonal and daily variations of the atmospheric refractivity (year 2005 - 2010 in Vilnius) [IP5].

However, instantaneous variations of the radio refractivity are not so smooth. One-day measurements[4] are presented in Figure 5.

[3] Collected from the national weather stations and freely available archives, such as https://www.wunderground.com/.

[4] The measurements were carried out in Vilnius, on 8th April, 2015. No precipitation were observed.

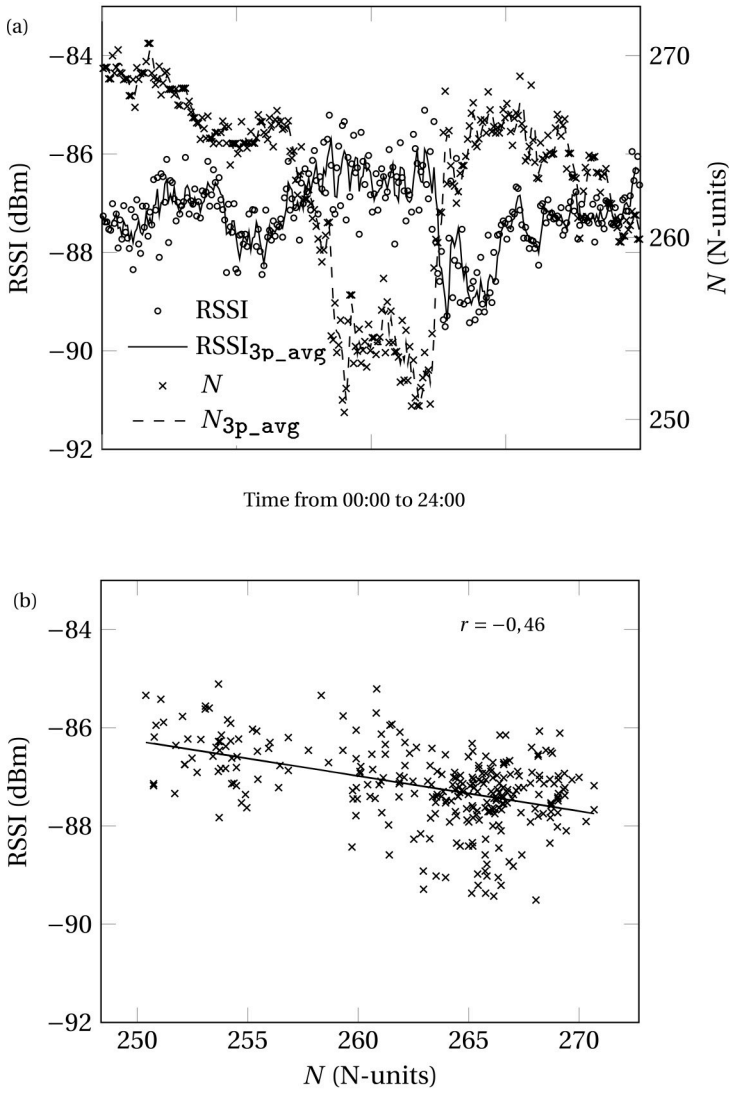

Figure 5. (a) Comparison of the *N*-value (in *N*-units) and the measured RSSI value (in dBm) (3.5 GHz frequency); measurements were carried out in the area of the poor coverage. Essential signal changes occur at the same time as the refractivity changes; (b) Linear regression of the *N* and RSSI values (a moderate negative correlation) (data from [PS1]).

The *N*-values were calculated in 10-minute intervals using real-time meteorological data, measured using WS1080 local weather station. The measured Received-Signal-Strength-Indicator (RSSI) values of the 3.5 GHz (WiMAX) signal are presented as well. The measurements of the meteorological data and the RSSI values were carried out in the same time and place, in the area of the poor coverage. As can be seen in the Figure 5, the essential signal changes occur at the same time as the refractivity changes.

Another subject of the study is atmospheric refractivity gradient, *G*. In measurements carried out in Kaunas (2009 – 2011) [IP6], [IP4] the temperature inversion, super-refraction and ducting layers were observed.

Sometimes there is no possibility to measure required meteorological parameters in the locations of interest. Therefore, a new model was proposed in [IP3]. It is based on the three known points outside the location of interest. In this case, unknown atmospheric refractivity value, W, could be calculated mathematically (Eq. (7-11)), knowing the coordinates of these three points (see Figure 6).

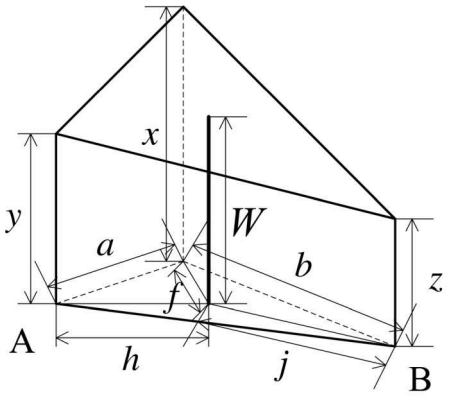

Figure 6. Model based on the three known points outside the location of interest [IP3]

$$W = z + \frac{t-(t-d)f\frac{\sin(\pi-\zeta)}{a\sin\zeta}}{f\frac{\sin\vartheta}{\sin(\pi-\zeta)}+j}, \tag{7}$$

here ζ, ϑ, t, d are:

$$\zeta = \cos^{-1}\left(\frac{j^2+f^2-b^2}{2f}\right), \tag{8}$$

$$\vartheta = \cos^{-1}\left(\frac{a^2+f^2-h^2}{2fa}\right), \tag{9}$$

$$t = x - z, \tag{10}$$

$$d = y - z. \tag{11}$$

The aforementioned findings allowed to formulate the following statement for defense:

Modelling of the electromagnetic wave attenuation in the atmosphere in the case of the 5G/B5G networks, requires the instantaneous (“one minute”) rain-rate and refractive index values, since averaged data may lead to significant deviations from the real values.

2. Simulations using the classical scattering theory

The purpose of this part is to theoretically examine the expected peculiarities of THz wave attenuation due to rain in case of short range communications and quasi-optical transmission (such scenarios will most probably be necessary to provide high bit-rates with sub-THz and THz carrier frequencies) [IP2]. This will also reduce the volume in which the interaction between the THz waves and rain droplets occurs. In turn, this might mean substantial deviations [27], [28] of instantaneous absorption from well-known averaged attenuation models. Calculations were performed emulating both drop size distributions of the real rain and the laboratory controlled rain described in literature sources.

2.1. Simulation methods

The classical scattering theory for a plane wave radiation by an absorbing sphere particles [33] is widely used (including [6], [11], [27], [28]) tool for the detailed analysis of attenuation in the THz range. Rain attenuation coefficient α (in dB/km) within this theory can be calculated as:

$$\alpha = 4.343 \int_0^\infty N(D) Q_t(D, \lambda, m) \mathrm{d}D, \tag{12}$$

$$Q_t(D, \lambda, m) = \frac{\lambda^2}{2\pi} \sum_{n=1}^{\infty} (2n+1)\, \mathrm{Re}[a_n + b_n], \tag{13}$$

here D is a raindrop diameter, $N(D)$ is a raindrop size distribution, $Q_t(D, \lambda, m)$ is an attenuation cross-section of a raindrop, λ is a wavelength, m is the complex coefficient of refraction for water, a_n and b_n are the Mie scattering coefficients, and 4.343 factor is used to obtain values in dB per unit distance. Values of m in sub-THz and THz ranges were taken from [34], and the Mie scattering coefficients were calculated using Matlab functions from [23], [35]. Weibull distribution and coefficients from [27], [28] were used to evaluate $N(D)$:

$$N(D) = N_0 \frac{c}{b} \left(\frac{D}{b}\right)^{c-1} e^{-\left(\frac{D}{b}\right)^c}, \tag{14}$$

here $N_0 = 1000$ m^{-3}, $b = 0.26R^{0.44}$ mm, $c = 0.95R^{0.14}$ and R is the rain-rate (in mm/h).

Two data transmission scenarios were considered. First, the relatively large distance ("Terahertz wall"[5] at $L = 100$ m), quasi-optical transmission and uniform beam shape between the antennas; and second, quasi-optical transmission at short distances ($L = 4$ m for easier comparison with the results of the laboratory-controlled rain [11]).

2.2. Simulation results

The distributions of raindrop sizes (presented in Figure 7(a)) were obtained from Eq. (14) for several rain-rates of heavy rain. The complex coefficient of refraction of water and attenuation cross-sections (also Figure 7(a)) were calculated for temperature $t = 20°C$ and $f = 0.3$ THz frequency. Contributions by rain drops of various sizes to the rain attenuation coefficient (Eq. (12)) are presented in Figure 7(b).

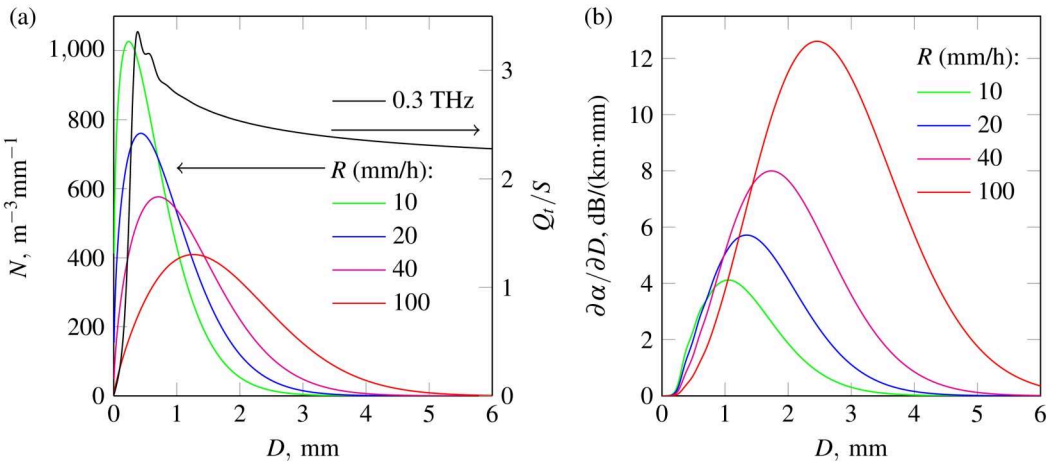

Figure 7. (a) Distributions of raindrop sizes for several rain rates R; the dependence of Q_t and raindrop cross-section area $S = \pi \cdot D^2/4$ ratio on the diameter of the raindrop for $f = 0.3$ THz frequency. (b) Dependence of the contribution to the averaged absorption coefficient on the diameter of the raindrop at $f = 0.3$ THz for several rain rates R [IP2].

As can be seen, the contribution of the small drops ($D < 0.2$ mm) to the overall loss is low even for lowest rain-rate $R = 10$ mm/h with highest concentrations of small

[5] Transmitting at distances of less than 100 meters is the only way to avoid the "Terahertz wall" (power needed to send data at terahertz frequencies would be impractically high in many cases) **Invalid source specified.**.

drops. For higher R-values, larger drops of $D > 0.2$ mm start to dominate both in terms of concentrations and contributions to the overall loss.

In the case of the first scenario, interaction with raindrops within large volume of $V \approx 100$ m^3 order and independently appearing raindrops are assumed. Even for narrow ranges of raindrop diameters $\Delta D = 0.01$ mm, average number of raindrops in such size intervals would reach tens and hundreds for most sizes of interest. In such conditions, Poisson distribution could be approximated by normal distribution with probability density function. Loss α_i induced by rain drops in the i-th interval can be evaluated using Eq. (12), divided by volume V in which interaction between the wave and raindrops occurs, and multiplication by ΔD can replace the integration for small ΔD, and thus α_i is also normally distributed with the mean $\bar{\alpha}_i$. Then the variance is:

$$\sigma_i^2 = \left(4.343 Q_t(D_i, \lambda, m)\right)^2 N(D_i) \Delta D / V = \mu_i^2 / N(D_i) V \Delta D. \quad (15)$$

Within the model of independent raindrops, absorption coefficient α_r for wider ranges between i_1 and i_2 can be expressed as:

$$\alpha_r = \sum_{i=i_1}^{i_2} \alpha_i, \quad \bar{\alpha}_r = \sum_{i=i_1}^{i_2} \bar{\alpha}_i, \quad \sigma_r^2 = \sum_{i=i_1}^{i_2} \sigma_i^2. \quad (16)$$

Nevertheless, an explicit $\sigma_i \propto V^{-1/2}$ dependence in Eq. (15) means that one should expect numerical values of $3\sigma_r$ uncertainties to grow into tens of percent of the average value once $V \approx 1$ m^3 beam-rain interaction volumes are approached. Such values, however, are exactly of the same order as ones discussed for ultra-dense outdoor 5G networks [35] and thus influence of the absorption coefficient deviations will have inevitably be considered for 5G.

The second scenario and comparison with the experimental data of [11] brings additional challenges. Small volume and Figure 7(a) data mean that average number of rain drops interacting with the wave might be well below 1 for each i. Thus, Poisson statistics was employed instead of normal distribution approximation. In addition, influences of multiple measurement (1000 in [11]) averaging and influence of more uniformly distributed drop sizes of the experimental set up have to be assessed. Results of such emulated measurements representing 1000 numerically generated rain drop size distributions within the communication channel are presented in Figure 8. A slight

difference between $\alpha_r \cdot L$ and $\bar{A}$ can be noticed suggesting that 1000 sets of rain drops (or data points for averaging in the experiment) is still insufficient to obtain a precise value of the average absorbance. To verify this assumption, simulated experiment was repeated 100 times (with 1000 measurement averaging in each) and distribution of $\bar{A}$ is presented in Figure 8(b).

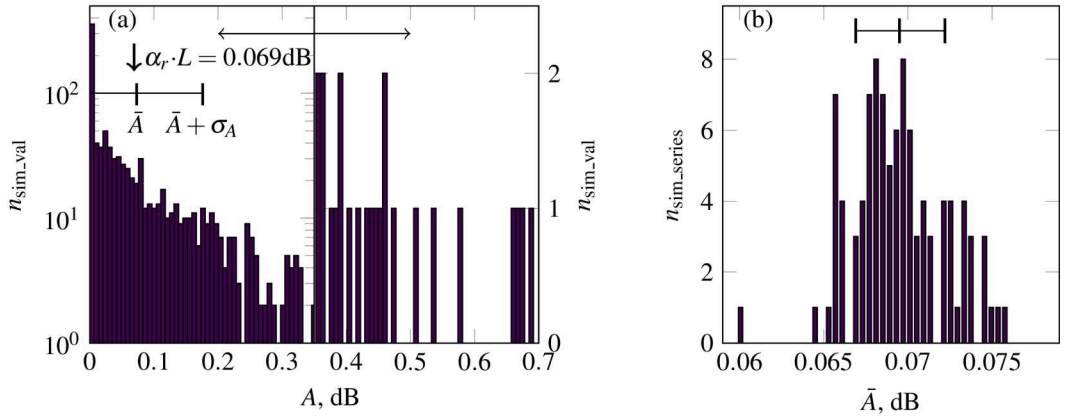

Figure 8. (a) Distribution of 1000 simulated absorbance A values at $R = 40$ mm/h rain rate, $f = 0.3$ THz frequency and Weibull distribution of drop sizes. Graph is split in the middle to reveal better lower numbers of $n_{\text{sim\_val}}$ (emulated single "measurements") with high absorbances. Bar width equals 0.007 dB. Average expected absorbance of $\alpha_r \cdot L = 0.069$ dB is indicated by an arrow in the same figure. (b) Distribution of the average values of A, obtained in simulated 100 absorbance data set series by averaging 1000 absorbance values within each set. Similarly to (a), central vertical line indicates the obtained average and two others - standard deviation from the average for such series ($\pm\sigma_{\bar{A}}$) [IP2].

The same numerical experiment series was repeated for the same 0.069 dB average loss, but with single allowed diameter of the drops $D = 1.9$ mm to evaluate the possible influence of more homogeneous drop sizes on the standard deviation. Calculated standard deviation in case of one single experiment was slightly smaller in comparison with Figure 8(a). On the other hand, average value for 100 experiment series and its' standard deviation are very close to the one obtained in Figure 8(a), confirming that larger series of substantially more than 1000 measurements would probably lead to very similar statistical results despite the size restrictions. An additional series of experiments were performed for average absorbance of 0.69 dB, corresponding to a case of an extreme rain. Dispersion is reduced about 30 times (when normalized to the average value), as expected when the average number of interacting rain drops increases. Furthermore, after additional

experiment series the results agreed with the experiment of the laboratory controlled rain, thus, confirming that laboratory-based experiments could be a valuable tool for estimating the upper limit of rain induced noise in communication channels despite of rain drop size distribution differences.

The aforementioned finding allowed to formulate the following statement for defense:

> Due to the quasi-optical transmission and relatively short distances of the 5G/B5G wireless networks (in relation to today's wireless communications), the attenuation deviations can be noticeable from values based on today's standardized models.

3. Simulation of the anti-reflective and phase-shifting compact optical elements for terahertz frequency band

As it was mentioned in the introduction part, simulation of the atmospheric attenuation is just one of the steps in the development of THz telecommunications. The other step is the system components that will support the basic principles of the 5G/B5G technology under very high absorption and scattering conditions. Therefore, one of the tasks of this work was to simulate anti-reflective and radiation phase-shifting compact elements for the THz spectral band. The results were used to create a zone plate design, in which reflection-reducing and focusing features are compatible and all of this comes on one 500 μm thick silicon substrate.

Zone plates are a type of the focusing elements that perform a phase shift function [36] and are thinner than the standard focusing elements [14], [37] , therefore, could replace the convex lenses in the THz antennas. The idea of the zone plate antenna was described both for 5G and B5G technologies at [16], [14], [17]. It was concluded in [14], that the zone plates are more compact in terms of depth, volume and weight.

This work emphasizes the design of the zone plane, combining both reflection-reducing and phase-shifting properties, as well somewhat unusual laser production method (compared to etching [38], [39], [40]). Binary focusing zone plate for 0.6 THz frequency was designed, produced and its focusing performance was evaluated. Nearly diffraction limited performance was obtained.

3.1. Optimization of anti-reflective structures for laser processing

Two types of anti-reflective (AR) layers were first investigated and compared: one with the vertical side-walls, which could potentially be obtained by means of anisotropic or deep inductive plasma etching (DRIE), and the other one with the sloped side walls, optimized for laser micro-machining. Their initial thickness was estimated to be approximately equal to the quarter wavelength of 0.6 THz radiation at the interim effective refractive index between air and silicon. Simulations were performed using MIT Meep [41] software package. For an infinite 2D array of repeating elements, propagation of

waves within only one segment was simulated, and Bloch-periodic boundary conditions were applied on the side-walls of the segment. Propagation of a pulsed THz wave was simulated in order to obtain the whole reflectance spectrum within one simulation.

First of all, vertical side-wall AR coating was investigated. The same fill factor (FF, ratio of the remaining silicon volume to the total volume of the layer) of $FF = 0.64$ and variable period of the structure ($L = 50; 100; 150$ μm) revealed several frequency- and size-dependent features. The simulation results are presented in Figure 9(a). Thereafter, structures with the 100 μm period were investigated in more detail.

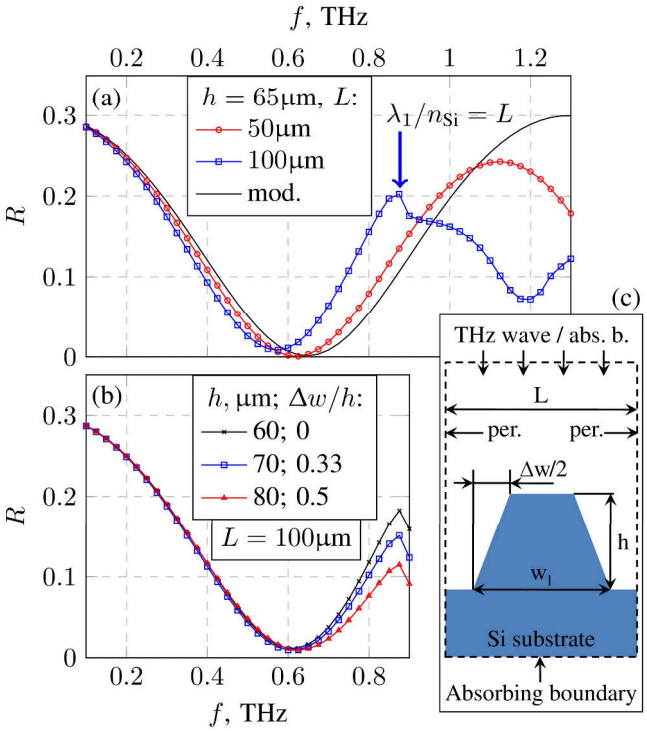

Figure 9. (a) Calculated reflectance spectra of three coatings of the same depth $h = 65$ μm, $FF = 0.64$ and $w/L = 0.8$, but different periods L. For comparison purposes, an analytical solution based on a simplified equivalent circuit model for the effective dielectric constant evaluation [38] is also presented (black line). (b) Results of simulations for a fixed position of reflectance minimum and adjusted height h and side wall slope (d). Si pyramid base width w_1 was increasing when specifying sloped side walls to maintain the averaged within AR structure fill factor of $FF = 0.64 \pm 0.01$. Simulations were performed for a semi-infinite substrate in order to emphasize properties of a single AR structure. (c) Sketch of the structure with sloped side-walls with indicated parameters used for further describing simulations. Dashed line indicates a contour of the structure with a vertical side wall. [IP1]

Due to the focusing of the laser beam, perfectly vertical walls are hardly possible, therefore, structure with sloped side-walls (see Figure 9(c)) was chosen. Several additional

series of simulations were performed with similar $FF = 0.64 \pm 0.01$, but different side-wall slope. For a fixed depth h, the reflectance minimum shift to higher frequencies once the slope increases has to be compensated by the increase of the depth h. Once the Si pyramid width at the base w_1 approaches the period of the structure L, an effective refractive index of the structure approaches that of bulk Si thus reducing the contribution of this area to distributed reflections. No significant distortions of the spectrum due to the slope of the side walls were expected.

So far, a semi-infinite (that is, one side is infinite) substrate was assumed. The situation becomes more complex once the finite thickness of the substrate and option of the second structured surface are considered. In addition, fabrication tolerances have to be taken into account. Thus, much thicker AR structures were selected for fabrication. AR structures were fabricated on both sides of high resistivity float-zone (FZ) Si wafers to obtain the best performance. Fixed period of $L = 100$ μm was selected based on the previously discussed optimization be means of finite-difference time-domain (FDTD) simulations.

3.2. THz time-domain spectroscopy (THz-TDS) measurements

Transmittances of the samples were studied using Ekspla-Teravil THz-TDS spectroscopy and THz imaging system. Two-dimensional scan was performed in order to check whether irregularities of pyramid shapes led to irregularities of transmittance. The results are presented in Figure 10.

Table 1. Parameters of ablated AR structures and their theoretical approximations [IP1]. A – numerically simulated, E - experimentally investigated.

Ablated structure	Structured sides	Simulated structure	Approximation parameters
B_{2E}	Yes	B_{2A}	$h = 100$ μm, $w_1 = 75$ μm, $\Delta w/h = 0.25$ μm
B_{3E}	Yes	B_{3A}	$h = 195$ μm, $w_1 = 100$ μm, $\Delta w/h = 0.33$ μm

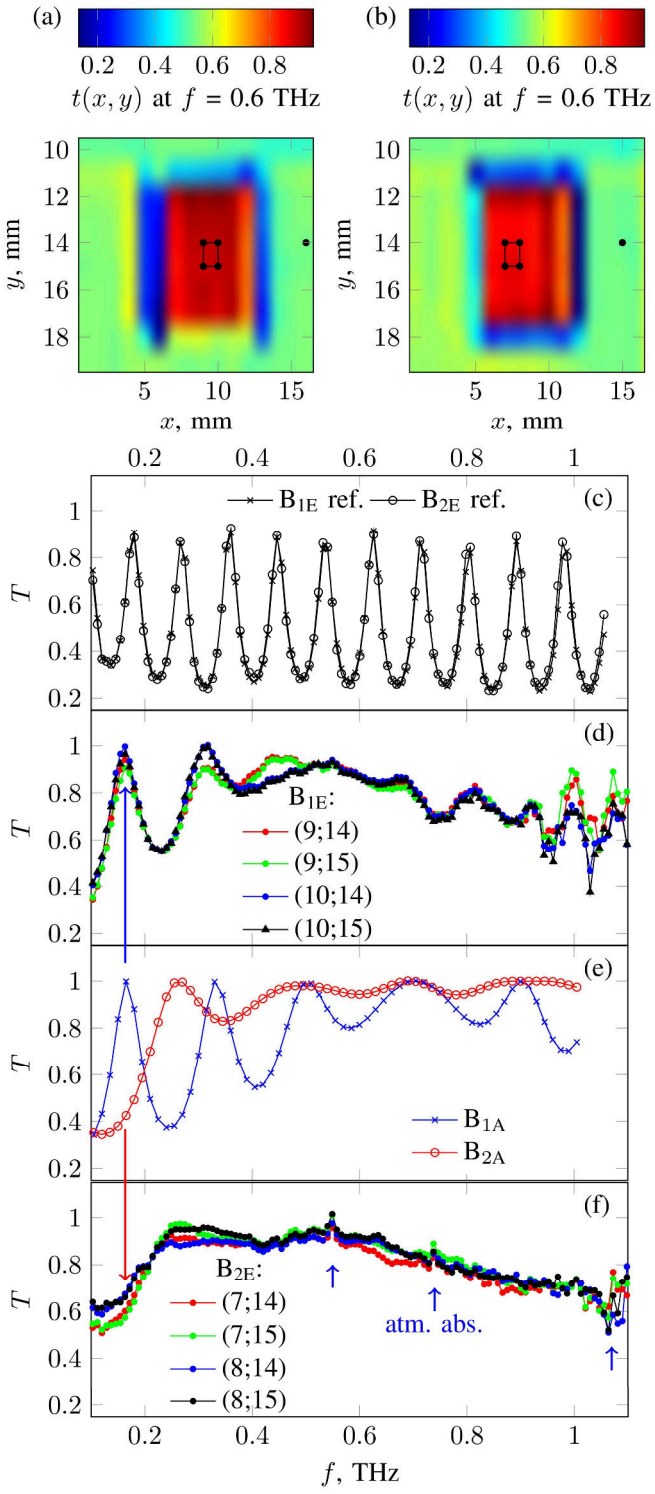

Figure 10. Distribution of amplitude transmission coefficient t for samples B_{2E} (a) and B_{3E} (b) at 0.6 THz frequency. Rightmost black points indicate positions of flat unprocessed wafer reference areas for which transmittance spectra are presented in panel (c). Rectangles and points at their corners in (a) in (b) indicate the positions of AR structure for which transmittance spectra are presented (d), and (f) respectively. Two simulated transmittance spectra for wafers with B_{2A} and B_{3A} structured surfaces on both sides (parameters are listed in Table 1) are presented in (e). Measurement errors due to the influence of atmospheric absorption lines are indicated in (f) by vertical blue arrows [IP1].

Two points of the flat wafer and four points near the middle of the structured part (indicated by black points) of the sample B_{2E} (see Table 1) were investigated in detail. Transmittance spectra for two points of the flat wafer (Figure 10(c)) nearly perfectly match the one expected for 500 μm thick HR Si wafer. Transmittance spectra obtained at 4 points near the middle of the structured area of sample B_{2E} are presented in Figure 10(d). Disappearance of interference fringes and stable transmittance of $T \approx 0.9$ in a vicinity of 0.5-0.6 THz confirms efficiency of the produced AR layer. This finding is consistent with simulation results for B_{2A}. This indicates that the average amount of a removed material was correctly estimated for modelling and small local effective thickness variations do not introduce substantial differences between the phase shifts between the measurement locations[6].

3.3. Phase shift performance of AR structures

Dependences of normalized electric field on time for THz pulses to be transmitted through samples B_{2E} and B_{3E} are presented in Figure 11.

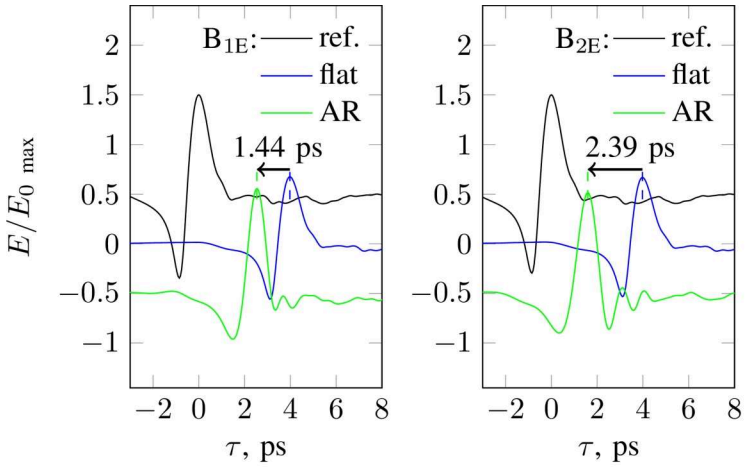

Figure 11. Dependence of normalized electric field on time for three pulses: reference (”ref.”), transmitted through a flat area of the wafer (”flat”) and transmitted through the structured sample area (”AR”). Pulse delay differences between flat and structured areas of the sample are indicated by arrows [IP1].

[6] Larger phase shift differences due to local variations at higher frequencies are not substantial enough to prevent an efficient operation of the binary zone plate.

Delays of the pulses are reduced in both areas of the samples with AR structures due to Si removal and reduction of the effective refractive index (reduction by 1.44 ps and 2.39 ps in B_{2E} and B_{3E}, respectively; the difference of 0.95 ps corresponds to approximately 57% of the period for 0.6 Hz and half for 0.53 THz). Such result opens a possibility for a future implementation of such layers in, for example, high efficiency zone plates at THz frequencies, ensuring thus both required phase shifts between zones and high transmittance.

Further thinning of the remaining unstructured middle part of substrates is one of the most obvious ways to further reduce pulse delays and achieve full 2π phase shifts in comparison with thinner B_{2E} coating. Complete replacement of 110 μm thick Si with air would be enough for efficient wave front management at a given frequency, however, the mechanical stability of the Si film holding AR structures would suffer dramatically. Therefore, additional FDTD simulations were employed. The results are presented in Figure 12. Several calculated reflectance spectra are presented as well.

Nearly uniform amplitude distributions and only marginal wave front distortions are visible at $z < -200$ μm, confirming that there is no scattering despite relatively large sizes of pyramids. Also, the expected phase shift differences can be calculated from positions of electric field maxima (indicated by arrows). The 15 μm difference in Si and narrowing of pyramid base by 15 μm would eliminate the difference to 1λ. Reflectance spectra revealed that even at 85 μm width, no significant reflectivity increase is expected, therefore, such width would be sufficiently small to achieve a shift of full wave.

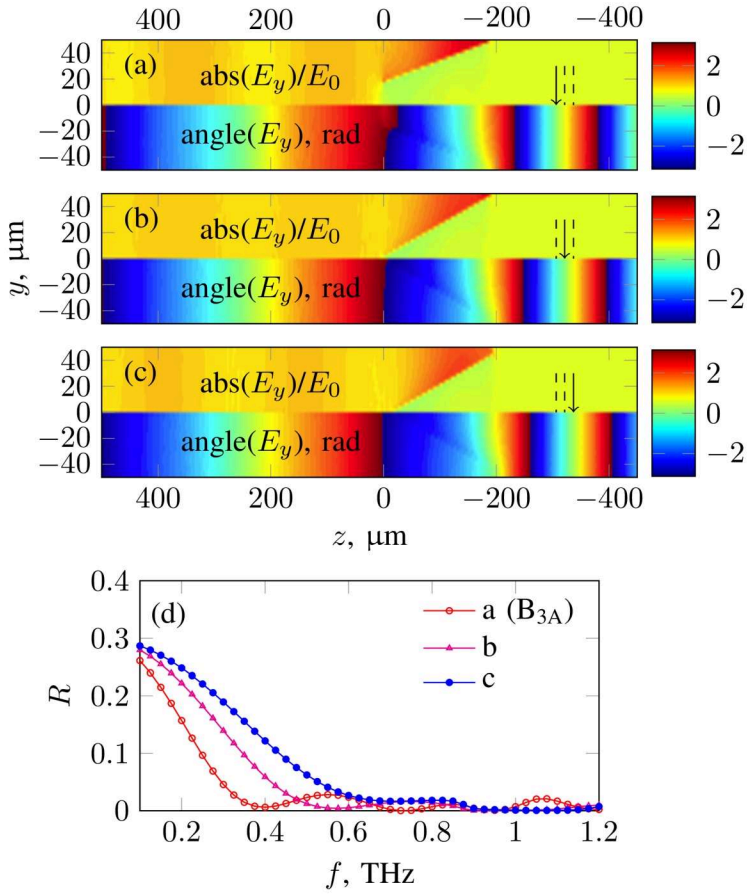

Figure 12. Simulated distributions of electric field component E_y for 3 AR structures (a-c) on a semi-infinite substrate and reflectance spectra of the structures (d). Amplitude data are presented in the upper parts ($y > 0$) of the panels (a-c) and phases of E_y - in lower ($y < 0$) ones. Arrows and dashed lines indicate maxima positions of a real part of the electric field within the substrates in panels (a-c) [IP1].

3.4. Focusing performance of AR structures based on the phase shifts

Prototype binary zone plate (ZP) for 0.6 THz frequency and $F = 5$ mm focal length was produced aiming to verify whether phase-shifting properties of AR structures are sufficiently uniform for focusing applications.

Alternating rings with either flat or structured surface were formed on the one side of the same highly resistive Si wafer of 500 µm thickness (Figure 13). B_{2E} design served as a basis for the AR structure, whilst amount of removed Si was increased by approximately 10% to obtain π phase shift at 0.6 THz when compared to flat surface. The another side of the wafer was uniformly structured to reduce the influence of the reflections.

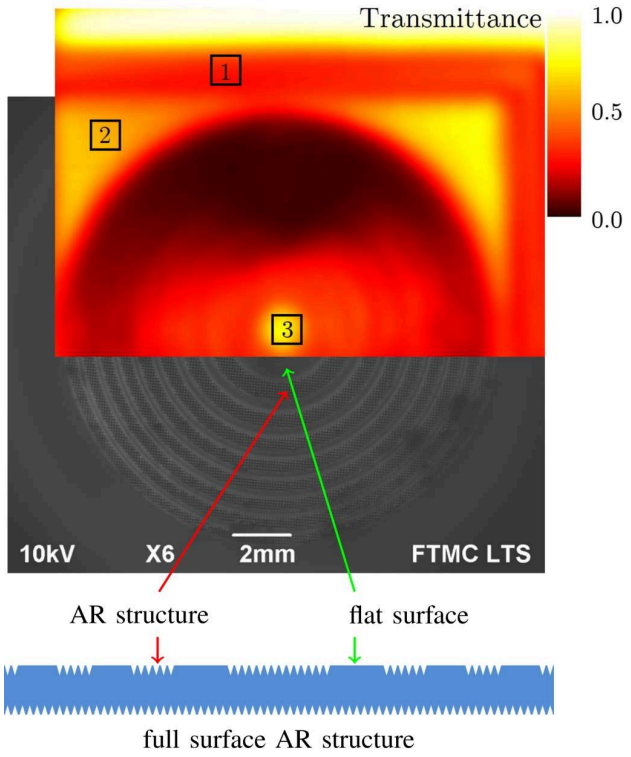

Figure 13. SEM and THz transmittance (at $f = 0.6$ THz) images (top) and sketch (bottom, not to scale) of the prototype zone plate. Alternating zones with either flat or structured surfaces are seen in SEM image. ZP was placed a sample in the focal point of the continuous wave (CW) THz imaging system with pyroelectric sensor to obtain the presented transmittance map. Three regions of interest are shown in THz image: flat silicon with approximately 30% transmittance (1), silicon with one AR structured surface and approximately 60% transmittance (2) and center of ZP with maximum transmittance of 76% [IP1].

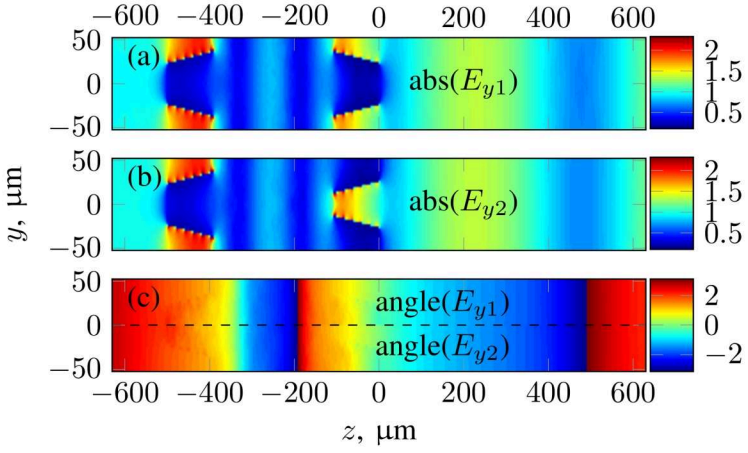

Figure 14. Distributions of electric field amplitude in case of matching positions of pyramids on both surfaces (a) and in case of shifted by half of period pyramids on the front surface (b). Values were divided by the amplitude of the incident wave. Phase distributions in both cases are presented in the same panel (c) for an easier comparison. The upper part ($y > 0$) is dedicated to the case with matching pyramid positions and the lower part - to the position mismatch case. Assumed ablation depth was increased to 110 µm to match better the structure later used for the zone plate [IP1].

Two additional simulations were made to compare the cases of matching pyramid positions and of the shift by half of the period. Both amplitude and phase distributions for these two cases are presented in Figure 14. No essential phase differences can be observed both in the middle of the substrate and outside the sample. It thus confirms that very exact pyramid position match between the layers is not required.

Focusing performance of the incident THz waves was evaluated by imaging of the spatial beam profiles of THz radiation. The distance between the THz source and zone plate was approximately 1 meter. Initially, the profile of collimated THz beam was measured (Figure 15(b)), then the spatial profile measurements were repeated with the zone plate inserted at the focal distance from the detector (Figure 15(c)).

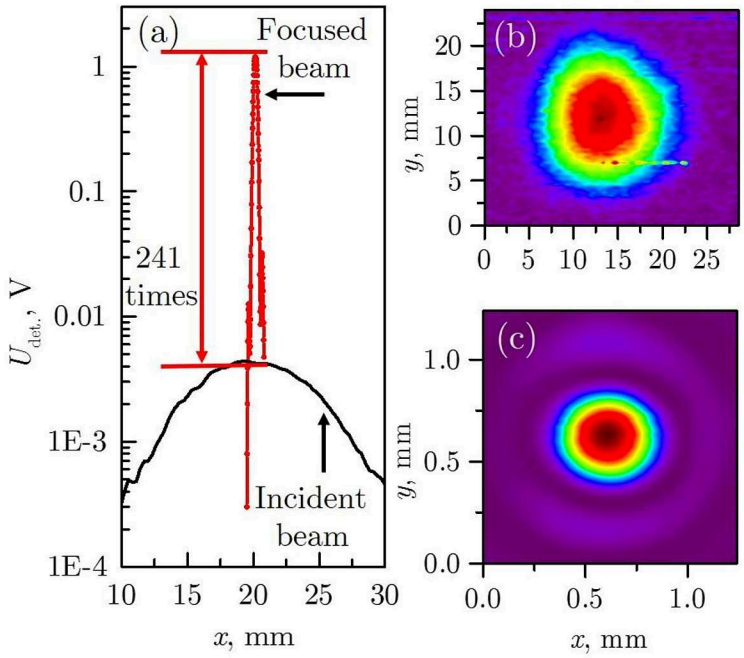

Figure 15. Cross-sections of the beam profiles of the incident wave and the focused one through the maximum point (a). First dependence of detector signal on coordinates was recorded when it was illuminated with a collimated THz beam (b). Afterwards, zone plate was inserted, and measurements were repeated at the focal plane with higher resolution (c) [IP1].

Cross-sections are presented in (Figure 15(a)) for easier comparison. Presented data confirms that maximum signal increase of approximately 240 times is obtained and full-

width at half-maximum below one wavelength is evaluated even though relatively narrow incident wave spans just several Fresnel zones of the zone plate. Therefore, binary zone plate can successfully be used for focusing and uniformity of the fabricated AR structures is sufficient to obtain nearly diffraction limited performance.

The aforementioned finding allowed to formulate the following statements for defense:

- In the reflection-reducing layers, where the period of the structure is close to the incident wavelength, it is possible to produce a thinner antireflective layer and to ease the production of the layers using laser-ablation method, while maintaining a small reflection coefficient.
- Phase shifts in such structured reflection-reducing layers made of silicon are sufficiently well controlled, therefore, high quality focusing elements could be obtained for both THz telecommunication and THz imaging systems, allowing to reach close to diffraction limited operation.

Main results and conclusions

1) Modelling of the electromagnetic wave attenuation in the atmosphere in the case of the 5G/B5G networks, requires the instantaneous ("one minute") rain-rate and refractive index values, since averaged data may lead to significant deviations from the real values.
    a. It was demonstrated for sub-THz (100 GHz) and THz (300 GHz) frequencies that averaged rain-rate values on heavy-rain conditions distort the results: the decrease of large values, the increase of small values and shifts in time were observed;
    b. In the area of the poor coverage changes of the signal strength occurred at the same time as variations of atmospheric refractive index with a moderate negative correlation ($r = -0.46$).
    c. A model for calculation of the atmospheric refractivity, when there is no possibility to measure required meteorological parameters in the locations of interest, was suggested.
2) Due to the quasi-optical transmission and relatively short distances of the 5G/B5G wireless networks (in relation to today's wireless communications), the attenuation deviations can be noticeable from values based on today's standardized models.
    a. Calculations of the expected absorption coefficient deviations for the THz frequency band and quasi-optical transmission in short-range scenario, that can be expected in the B5G networks, revealed, that deviations are significant compared to the average, and in some cases (i.e., laboratory-controlled rain) it can be exceeded.
3) In the reflection-reducing layers, where the period of the structure is close to the incident wavelength, it is possible to produce a thinner antireflective layer and to ease the production of the layers using laser-ablation method, while maintaining a small reflection coefficient.
    a. On the basis of this finding, reflection-reducing AR layers were designed and optimized for production using laser-ablation method.

b. Inevitable shape imperfections, occurring due to physical processes during laser processing can be compensated by the increase of the depth.
c. Transmittance reaching about 90% was obtained within 0.5 - 0.6 THz for Si wafers with both structured surfaces.

4) Phase shifts in such structured reflection-reducing layers made of silicon are sufficiently well controlled, therefore, high quality focusing elements could be obtained for both THz telecommunication and THz imaging systems, allowing to reach close to diffraction limited operation.
   a. Peculiarities of the phase shift in the reflection-reducing AR layers and possibilities to use them for focusing elements directly on the on the semiconductor substrates were investigated;
   b. The phase-shifting possibilities were employed for the zone plate design, in which reflection-reducing and focusing features (2π phase shift, maximum signal increase of approximately 240 times) are compatible on one 500 μm thick silicon substrate.

References

[1] S. Cherry, "Edholms law of bandwidth", *IEEE Spectrum,* vol. 41, pp. 58-60, 2004.

[2] Ericsson, „Traffic exploration tool", 2017. Online: https://www.ericsson.com/TET/trafficView/loadBasicEditor.ericsson.

[3] C. E. Shannon, "Communication in the presence of noise", *Proceedings of the IRE,* vol. 37, pp. 10-21, 1949.

[4] Bell Labs Consulting, „Who will satisfy the desire to consume? How will wireless data demand grow between now and 2020 and how should mobile operators respond?", 2016. Online: https://readymag.com/BellLabs/480968/.

[5] Y. S. Lee, Principles of terahertz science and technology, Springer Science & Business Media, 2009.

[6] J. Federici and L. Moeller, "Review of terahertz and subterahertz wireless communications", *Journal of Applied Physics,* vol. 107, p. 111101, 2010.

[7] N. Kukutsu, A. Hirata, M. Yaita, K. Ajito, H. Takahashi, T. Kosugi, H. Song, H. Wakatsuki, Y. Muramoto, T. Nagatsuma and Y. Kado, "Toward practical applications over 100 GHz", *2010 IEEE MTT-S International Microwave Symposium,* pp. 1134-1137, 2010.

[8] K. Ishigaki, M. Shiraishi, S. Suzuki, M. Asada, N. Nishiyama and S. Arai, "Direct intensity modulation and wireless data transmission characteristics of terahertz-oscillating resonant tunnelling diodes", *Electronics Letters,* vol. 48, p. 582, 2012.

[9] A. C. K. Nordrum, „Everything You Need to Know About 5G", 2017. Online: https://spectrum.ieee.org/video/telecom/wireless/everything-you-need-to-know-about-5g.

[10] T. Nagatsuma, G. Ducournau and C. C. Renaud, "Advances in terahertz communications accelerated by photonics", *Nature Photonics,* vol. 10, pp. 371-379, 2016.

[11] J. Ma, F. Vorrius, L. Lamb, L. Moeller and J. F. Federici, "Comparison of experimental and theoretical determined terahertz attenuation in controlled rain", *Journal of Infrared, Millimeter, and Terahertz Waves,* vol. 36, pp. 1195-1202, 2015.

[12] S. Yost, „What Does Every Engineer Need to Know about 5G?", Online: https://spectrum.ieee.org/semiconductors/design/what-does-every-engineer-need-to-know-about-5g.

[13] I. F. Akyildiz, J. M. Jornet and C. Han, "Terahertz band: Next frontier for wireless communications", *Physical Communication,* vol. 12, pp. 16-32, 2014.

[14] J. M. Rodríguez, H. Hristov and W. Grote, "Fresnel zone plate and ordinary lens antennas: Comparative study at microwave and terahertz frequencies", *2011 41st European Microwave Conference,* 2011.

[15] Y. Ji and M. Fujita, "Design and analysis of a folded Fresnel Zone Plate antenna", *International Journal of Infrared and Millimeter Waves,* vol. 15, no. 8, p. 1385–1406, 1994.

[16] M. R. D. Kodnoeih, Y. Letestu, R. Sauleau, E. M. Cruz and A. Doll, "Compact Folded Fresnel Zone Plate Lens Antenna for mm-Wave Communications", *IEEE Antennas and Wireless Propagation Letters,* vol. 17, pp. 873-876, 5 2018.

[17] M. I. B. Shams, Z. Jiang, J. Qayyum, S. Rahman, P. Fay and L. Liu, "A terahertz reconfigurable photo-induced fresnel-zone-plate antenna for dynamic two-dimensional beam steering and forming", *2015 IEEE MTT-S International Microwave Symposium,* 2015.

[18] D. M. Pozar, Microwave engineering, John Wiley & Sons, 2012.

[19] *The HITRAN2016 Molecular Spectroscopic Database.*

[20] International Telecommunication Union, „Recommendation P.1817 : Propagation data required for the design of terrestrial free-space optical links", 02/2012. Online: https://www.itu.int/rec/R-REC-P.1817/en.

[21] Y. Yang, A. Shutler and D. Grischkowsky, "Measurement of the transmission of the atmosphere from 02 to 2 THz", *Optics Express,* vol. 19, p. 8830, 4 2011.

[22] R. L. Freeman, Radio System Design for Telecommunications, John Wiley & Sons, Inc., 2007.

[23] N. Currie, Principles and Applications of Millimeter-Wave Radar, Artech House Radar Library, 1987.

[24] R. S. International Telecommunication Union, *Recommendation ITU-R P.838: Specific attenuation model for rain for use in prediction methods,* 2005.

[25] R. Oblack, „The Real Shape of Raindrops", 2017. Online: http://weather.about.com/od/cloudsandprecipitation/a/rainburgers.htm.

[26] E. Adirosi, L. Baldini, F. Lombardo, F. Russo, F. Napolitano, E. Volpi and A. Tokay, "Comparison of different fittings of drop spectra for rainfall retrievals", *Advances in Water Resources,* vol. 83, pp. 55-67, 2015.

[27] M. Sekine, S. Ishii, S. I. Hwang and S. Sayama, "Weibull Raindrop-Size Distribution and its Application to Rain Attenuation from 30 GHz to 1000 GHz", *International Journal of Infrared and Millimeter Waves,* vol. 28, pp. 383-392, 01 5 2007.

[28] S. Ishii, M. Kinugawa, S. Wakiyama, S. Sayama and T. Kamei, "Rain Attenuation in the Microwave-to-Terahertz Waveband", *Wireless Engineering and Technology,* vol. 7, p. 59, 2016.

[29] P. Rice and N. Holmberg, "Cumulative time statistics of surface-point rainfall rates", *IEEE Transactions on Communications,* vol. 21, pp. 1131-1136, 1973.

[30] F. M. L. Moupfouma, "Modelling of the rainfall rate cumulative distribution for the", *International Journal of Satellite,* vol. 13, no. 2, pp. 105-115, 1995.

[31] S. Okamura and T. Oguchi, "Electromagnetic wave propagation in rain and polarization effects", *Proceedings of the Japan Academy, Series B,* vol. 86, no. 6, p. 539–562, 2010.

[32] Internation Telecommunication Union, „Recommendation P.453-13: The radio refractive index: its formula and refractivity data", 12/2017. Online: https://www.itu.int/rec/R-REC-P.453/en.

[33] H. C. Hulst, Light scattering by small particles, John Wiley and sons, 1957.

[34] P. S. Ray, "Broadband complex refractive indices of ice and water", *Applied optics,* vol. 11, pp. 1836-1844, 1972.

[35] C. Mätzler, "MATLAB functions for Mie scattering and absorption, version 2", *IAP Res. Rep,* vol. 8, pp. 1-24, 2002.

[36] M. T. Barros, R. Mullins and S. Balasubramaniam, "Integrated Terahertz Communication With Reflectors for 5G Small-Cell Networks", *IEEE Transactions on Vehicular Technology,* vol. 66, pp. 5647-5657, 7 2017.

[37] P. Goldsmith, "Zone Plate Lens Antennas for Millimeter and Submillimeter Wavelengths", *The Third International Symposium on Space Terahertz Technology: Symposium Proceedings,* pp. 345-361, 1992.

[38] C. Kadlec, F. Kadlec, P. Kužel, K. Blary and P. Mounaix, "Materials with on-demand refractive indices in the terahertz range", *Opt. Lett.,* vol. 33, pp. 2275-2277, 10 2008.

[39] Y. W. Chen and X. C. Zhang, "Anti-reflection implementations for terahertz waves", *Front. Optoelectron.,* vol. 7, p. 243, 2014.

[40] Y. W. Chen, P. Y. Han and X.-C. Zhang, "Tunable broadband antireflection structures for silicon at terahertz frequency", *Appl. Phys. Lett.,* vol. 94, 2009.

[41] A. F. Oskooi, D. Roundy, M. Ibanescu, P. Bermel, J. D. Joannopoulos and S. G. Johnson, "MEEP: A flexible free-software package for electromagnetic simulations by the FDTD method", *Comput. Phys. Commun.,* vol. 181, pp. 687-702, 1 2010.

[42] C. M. Armstrong, „The Truth About Terahertz", 2012. Online: https://spectrum.ieee.org/aerospace/military/the-truth-about-terahertz.

List of ISI publications included in doctoral thesis

[IP1] **M. Tamošiūnaitė**, S. Indrišiūnas, V. Tamošiūnas, L. Minkevičius, A. Urbanowicz, G. Račiukaitis, I. Kašalynas, G. Valušis, Focusing of Terahertz Radiation with Laser-Ablated Antireflective Structures, *IEEE Transactions on Terahertz Science and Technology* [in press, DOI: 10.1109/TTHZ.2018.2859619].

[IP2] **M. Tamošiūnaitė**, V. Tamošiūnas, G. Valušis. Wireless Communications Beyond 5G: Uncertainties of Terahertz Wave Attenuation Due to Rain, Lithuanian Journal of Physics Vol. **58**, No. 2, 149–158 (2018).

[IP3] M. Zilinskas, **M. Tamosiunaite**, S. Tamosiunas, E. Brilius, M. Tamosiuniene, Model for Determination of Territorial Distribution of Surface Radio Refractivity, *Progress in Electromagnetics Research Symposium Proceedings*, *Stockholm, Sweden, Aug. 12-15*, *2013*, 1525-1529 (2013).

[IP4] M. Zilinskas*;* **M. Tamosiunaite**, M. Tamosiuniene, E. Valma, and S**.** Tamosiunas*;* Gradient of Radio Refractivity in Troposphere, *Progress In Electromagnetics Research Symposium Proceedings*, Moscow, Russia, August 19-23, 603-607 (2012).

[IP5] M. Žilinskas, S. Tamošiūnas, **M. Tamošiūnaitė**. M. Tamošiūnienė. Yearly, Seasonal and Daily Variations of Radio Refractivity, *Acta Physica Polonica A*, Vol. 119, No. 4, 533-536 (2011).

[IP6] E. Valma, **M. Tamosiunaite**, S. Tamosiunas, M. Tamosiuniene, M. Zilinskas, Variation of radio refractivity with height above ground, *Electronics and Electrical Engineering*, No. 5 (111), 23-26 (2011).

[IP7] **M. Tamošiūnaitė**, S. Tamošiūnas, V. Daukšas, M. Tamošiūnienė, M. Žilinskas. Prediction of electromagnetic waves attenuation due to rain in the localities of Lithuania. *Electronics and Electrical Engineering*, Nr. 9 (105), 9-12 (2010).

[IP8] E. Valma, **M. Tamošiūnaitė**, S. Tamošiūnas, M. Tamošiūnienė, M. Žilinskas. Determination of radio refractive index using meteorological data. *Electronics and Electrical Engineering*, Nr. 10 (106), 125-128 (2010).

[IP9] M. Žilinskas, **M. Tamošiūnaitė**, S. Tamošiūnas, M. Tamošiūnienė. The influence of the climatic peculiarities on the electromagnetic waves attenuation in the Baltic

Sea Region. *Progress in Electromagnetics Research Symposium Proceedings, March 24-28, 2008, Hangzhou, China*, Vol. 1, 227-231 (2008).

List of prepared publications included in doctoral thesis

[PS1] **M. Tamosiunaite**, S. Tamosiunas, M. Zilinskas, G. Valusis. Atmospheric Attenuation of the Terahertz Wireless Networks, in: Broadband Communications Networks - Recent Advances and Lessons from Practice, InTech.

Publications not included in the doctoral thesis

[NP1] M. Zilinskas, **M. Tamosiunaite**, S. Tamosiunas, M. Tamosiuniene, E. Stankevicius, The influence of atmospheric radio refractivity on the WiMAX signal level in the areas of weak coverage, in: *Proceedings of The 36th PIERS, Prague, Czech Republic, European Union, 6-9 July, 2015*

[NP2] **M. Tamošiūnaitė**, M. Žilinskas, M. Tamošiūnienė, S. Tamošiūnas. Atmospheric Attenuation due to Humidity. Chapter 8, pp. 157-172 // in: *Electromagnetic Waves*, Ed. Vitaliy Zhurbenko, ISBN: 978-953-307-304-0 (InTech, 2011)-510 p.

[NP3] **M. Tamošiūnaitė**, M. Tamošiūnienė, A. Gruodis, S. Tamošiūnas. Prediction of electromagnetic wave attenuation due to water in atmosphere. 1. Attenuation due to rain. *Innovative Infotechnologies for Science, Business and Education*, Vol. 2, No. 9, 3-10 (2010) ISSN 2029-1035.

[NP4] S. Tamošiūnas, **M. Tamošiūnaitė**, M. Žilinskas, M. Tamošiūnienė. The influence of fog on the propagation of the electromagnetic waves under Lithuanian climate condictions. *PIERS Online.* Vol. 5, No. 6 (2009).

[NP5] M. Žilinskas, **M. Tamošiūnaitė**, S. Tamošiūnas, M. Tamošiūnienė. Calculation of electromagnetic wave attenuation due to rain for various percentages of time. *Progress In Electromagnetics Research Symposium, Beijing, China, March 23–27, 2009 Proceedings,* 541-545 (2009).

[NP6] M. Žilinskas, **M. Tamošiūnaitė**, S. Tamošiūnas, M. Tamošiūnienė. The influence of the climatic peculiarities on the electromagnetic waves attenuation in the Baltic Sea Region. *PIERS Online*, Vol.4, No. 3, 321-325 (2008).

Presentations at the conferences

[C1] **M. Tamosiunaite**, S. Indrisiunas, V. Tamosiunas, L. Minkevicius, A. Urbanowicz, G. Raciukaitis, I. Kasalynas, G. Valusis, Laser-Ablated Antireflective and Phase Shifting Structures for Terahertz Range Optical Systems, *19-oji tarptautinė konferencija – mokykla "Advanced Materials and Technologies 2017", Palanga, 2018 m. rugpjūčio 27-31 d.* Programme: [https://advancedmaterials.ktu.edu/2017/doc/AMT2017_Programme.pdf].

[C2] **M. Tamošiūnaitė**, M. Žilinskas, S. Tamošiūnas, R. Rimkevičius, Atmosferos lūžio rodiklio įtaka radijo bangų signalo lygiui, *41-oji Lietuvos Nacionalinė fizikos konferencija, Vilnius, 2015 m. birželio 17-19 d.* Programme: [http://lnfk.ftmc.lt/wp-content/uploads/LNFK_PROGRAMA.pdf.].

[C3] **M. Tamošiūnaitė**, A. Gruodis, S. Tamošiūnas, Patikslintas blogiausio mėnesio modelis elektromagnetinių bangų slopai atmosferoje dėl vandens įtakos, *41-oji Lietuvos Nacionalinė fizikos konferencija, Vilnius, 2015 m. birželio 17-19 d.* Programme: [http://lnfk.ftmc.lt/wp-content/uploads/LNFK_PROGRAMA.pdf.].

[C4] **M. Tamošiūnaitė**, 4G interneto silpnybės ir galimi sprendimai, pritaikant RTD/SL sistemas, 4-oji doktorantų mokslinė konferencija FizTech, Fizinių ir Technologijos mokslų centras (2014).

[C5] M. Zilinskas, **M. Tamosiunaite**, S. Tamosiunas, M.Tamosiuniene, E. Stankevicius, The influence of atmospheric radio refractivity on the WiMAX signal level in the areas of weak coverage, The 36th PIERS, Prague, Czech Republic, European Union, 6-9 July, 2015.

[C6] M.Zilinskas, **M. Tamosiunaite**, S. Tamosiunas, E. Brilius, M. Tamosiuniene, Model for Determination of Territorial Distribution of Surface Radio Refractivity, *Progress in Electromagnetics Research Symposium, Stockholm, Sweden, Aug. 12-15*, *2013, Abstracts,* 1302 (2013).

[C7] A. Gruodis, **M. Tamošiūnaitė**, E. Valma, S. Tamošiūnas, Milda Tamošiūnienė, M. Žilinskas, Prediction of electromagnetic wave attenuation due to water in atmosphere. Variation of radio refractivity.5th International Conference Innovative information technologies for science, business and education IIT-2012, May 10-12, 2012, VILNIUS, Programme and Theses, p. 48 (Vilnius Business College, 2012).

[C8] M. Žilinskas, **M. Tamošiūnaitė**, M.Tamošiūnienė, E. Valma, S. Tamošiūnas, Gradient of radio refractivity in troposphere, *PIERS 2012 Moscow, Progress in Electromagnetics Research Symposium, Moscow, Russia, Aug. 19–23, 2012,* Program, p. 35

[C9] E. Valma, **M. Tamosiunaite**, S. Tamosiunas, M. Tamosiuniene**,** M. Zilinska**s.** Variation of radio refractivity with height above ground, *The 15th Int. Conf. on ELECTRONICS E 2011, May 17–19, 2011*, Kaunas and Vilnius, Lithuania.

[C10] **M. Tamošiūnaitė**, A. Gruodis, M. Tamošiūnienė, S. Tamošiūnas, Elektromagnetinių bangų silpninimas dėl kritulių įtakos (Electromagnetic wave attenuation due to influence of precipitation), *39-oji Lietuvos nacionalinė fizikos konf., skirta Rutherfordo atomo modelio 100 metų jubiliejui paminėti, Vilnius, 2011 m. sp. 6–8 d.:* Programme and Abstract, p. 254. ISBN 9789955634645. Programme: http://www.ff.vu.lt/sites/default/files/LNFK39_programa_0.pdf].

[C11] M. Žilinskas, S. Tamošiūnas, **M. Tamošiūnaitė**, M. Tamošiūnienė. *Determination of radio refractivity using meteorological data*. MIKON-2010: 4th Microwave & radar week MRW-2010, 18th International conference on microwaves, radar, and wireless communications: Vilnius, Lithuania, June 14-16, 2010. Vol. 2. Vilnius, 2010.

[C12] M. Žilinskas, **M. Tamošiūnaitė**, S. Tamošiūnas, M. Tamošiūnienė. *Determination of radio refractive index meteorological data*. 14th International conference on electronics: conference program: May 18-20, 2010, Kaunas and Vilnius, Lithuania. [S.l.], 2010.

[C13] **M. Tamošiūnaitė**, S. Tamošiūnas, M. Tamošiūnienė, M. Žilinskas. *Elektromagnetinių bangų silpninimas dėl lietaus Lietuvos vietovėse*. 38-oji Lietuvos nacionalinė fizikos konferencija: programa ir pranešimų tezės: Vilnius, 2009 m. birželio 8-10 d. Vilnius: Vilniaus universitetas, 2009.

[C14] M. Žilinskas, **M. Tamošiūnaitė**, S. Tamošiūnas, M. Tamošiūnienė. *Calculation of electromagnetic waves attenuation due to rain for various percentages time*. Progress in electromagnetics research symposium (PIERS 2009): abstracts, Beijing, China, March 23-27, 2009 Beijing, 2009.

[C15] M. Žilinskas, **M. Tamošiūnaitė**, S. Tamošiūnas, M. Tamošiūnienė. *The influence of the climatic peculiarities on the electromagnetic waves attenuation in the Baltic Sea region*. Progress in Electromagnetics Research Symposium (PIERS 2008), Hangzhou, China, March 24-28, 2008: abstracts. Cambridge (MA): The Electromagnetics Academy, 2008.

[C16] **M. Tamošiūnaitė**, S. Tamošiūnas, M. Tamošiūnienė, M. Žilinskas. *Influence of clouds on attenuation of electromagnetic waves*. Lithuanian Journal of Physics. Vol. 48, No. 1 (2008).

[C17] S. Tamošiūnas, **M. Tamošiūnaitė**, M. Tamošiūnienė, M. Žilinskas. *Attenuation due to rain for various percentages of time*. Radiation interaction with material and its use in technologies: International conference: Program and Materials. (2008).

[C18] **M. Tamošiūnaitė**, S. Tamošiūnas, M. Tamošiūnienė, M. Žilinskas. *Debesų įtaka elektromagnetinių bangų sklidimui*. 37-oji Lietuvos nacionalinė fizikos konferencija: programa ir pranešimų tezės, Vilnius, 2007 m. birželio 11-13 d. Vilnius: Vilniaus universitetas (2007).

About the author

Milda Tamošiūnaitė was born in 9 August, 1986 in Vilnius, Lithuania. She graduated from the Vilnius Viršuliškių (former 45th) secondary school in 2005. The same year she started studying at the Faculty of Physics of the Vilnius University, where she obtained Bachelor's diploma (2009, Physics; Physics and Management of Modern Technology) and Master's degree (2011, Physics; Atmospheric Physics and Chemistry). Milda started her doctoral studies in Physics (02P) at the at the Terahertz Photonics laboratory of the Center for Physical Sciences and Technology in 2012.